B2 and ALU retrotransposons are self-cleaving ribozymes whose activity is enhanced by EZH2

Alfredo J. Hernandez[a,1], Athanasios Zovoilis[b,c,1,2], Catherine Cifuentes-Rojas[b,c,1,3], Lu Han[b,c], Bojan Bujisic[b,c], and Jeannie T. Lee[b,c,4]

[a]Department of Biological Chemistry and Molecular Pharmacology, Harvard Medical School, Boston, MA 02115; [b]Department of Molecular Biology, Massachusetts General Hospital, Boston, MA 02114; and [c]Department of Genetics, The Blavatnik Institute, Harvard Medical School, Boston, MA 02114

Contributed by Jeannie T. Lee, November 18, 2019 (sent for review October 9, 2019; reviewed by Vivian G. Cheung and Karissa Y. Sanbonmatsu)

Transposable elements make up half of the mammalian genome. One of the most abundant is the short interspersed nuclear element (SINE). Among their million copies, B2 accounts for ∼350,000 in the mouse genome and has garnered special interest because of emerging roles in epigenetic regulation. Our recent work demonstrated that B2 RNA binds stress genes to retard transcription elongation. Although epigenetically silenced, B2s become massively up-regulated during thermal and other types of stress. Specifically, an interaction between B2 RNA and the Polycomb protein, EZH2, results in cleavage of B2 RNA, release of B2 RNA from chromatin, and activation of thermal stress genes. Although an established RNA-binding protein and histone methyltransferase, EZH2 is not known to be a nuclease. Here, we provide evidence for the surprising conclusion that B2 is a self-cleaving ribozyme. Ribozyme activity depends on Mg^{+2} and monovalent cations but is resistant to protease treatment. However, contact with EZH2 accelerates cleavage rate by >100-fold, suggesting that EZH2 promotes a cleavage-competent RNA conformation. B2 modification-interference analysis demonstrates that phosphorothioate changes at A and C nucleotides can substitute for EZH2. B2 nucleotides 45 to 55 and 100 to 101 are essential for activity. Finally, another family of SINEs, the human ALU element, also produces a self-cleaving RNA and is cleaved during T-cell activation as well as thermal and endoplasmic reticulum (ER) stress. Thus, B2/ALU SINEs may be classified as "epigenetic ribozymes" that function as transcriptional switches during stress. Given their high copy numbers, B2 and ALU may represent the predominant ribozyme activity in mammalian cells.

B2 | ALU | SINE | ribozyme | EZH2

Only 2% of the mammalian genome is protein coding (1–3). Originally viewed as "junk," the remaining 98% is increasingly recognized to play important roles in gene regulation and other crucial processes. Interestingly, approximately half of the noncoding genome is composed of transposable elements (4–6), the largest class of which is the retrotransposon. Retrotransposons can be subclassified into 1) endogenous retroviruses that contain long terminal repeats (LTRs), which are remnants of ancient retroviruses that invaded the genome (7), and 2) elements that lack LTRs, including the long interspersed nuclear elements (LINES) and short interspersed nuclear elements (SINEs) (8). SINEs, in particular, have garnered special interest in recent years because of their unusual behavior during times of organismal stress. SINEs originate from retrotransposition of RNA polymerase III transcripts, but to mobilize, they depend on LINE-encoded products for nuclease and reverse transcriptase activities (open reading frames 1 and 2) (9). In the mouse and human genomes, there are approximately 1 million SINE copies, which altogether account for ∼11% of the genomes. Because of their evolutionary age, SINEs have undergone extensive sequence changes and are now highly genetically diverse. In the mouse genome alone, for example, there are 4 subgroups of SINEs, including B1, B2, B4, and identifier (3). Among them, B2s have been most intensively studied.

B2s are present in ∼350,000 copies in the mouse genome (10) and give rise to 180- to 200-nucleotide (nt) polymerase III complex (POL-III) transcripts. B2 SINEs are transcriptionally active, with expression being highest in germ cells and in early development, after which they become epigenetically silenced. However, one of the most intriguing aspects of SINE biology is that these elements become highly up-regulated when somatic cells are acutely stressed (11–13), including during viral infection (8, 11), autoimmune processes such as macular degeneration (14, 15), and progression to cancer (16, 17). B2 expression is also sharply increased during thermal stress (18–21).

Thermal stress has proven especially informative for the investigation of B2 function. During the immediate early response to heat shock, B2 RNA is massively up-regulated. In vitro studies have shown that B2 RNA can incorporate into the RNA polymerase II complex (POL-II) and block formation of the preinitiation complex (20, 22). Our recent work showed that B2 RNA can also control transcription elongation by regulating pause–release of POL-II at promoter proximal positions (23) (Fig. 1*A*). Intriguingly, in the resting state, B2 RNA binds chromatin of stress response genes. Specifically, B2 binding to gene bodies suppresses transcription by forming "speed bumps" against

Significance

Among the 15 known classes of ribozymes, only 3 occur in mammals, and 6 are self-cleaving. Their physiological functions are mostly unclear. Here, we link a ribozyme activity to the stress response in mammals. We previously showed that the Polycomb protein, EZH2, induces cleavage of short interspersed nuclear element (SINE) B2 RNA to control the thermal stress response, but the nature of the nuclease activity was not known. We now demonstrate that RNAs made from 2 SINE retrotransposons, murine B2 and human ALU, are self-cleaving ribozymes and that EZH2 accelerates the reaction by 100-fold. We propose that B2/ALU SINEs are "epigenetic ribozymes" and that they represent two of the most abundant ribozyme activities in mammals.

Author contributions: A.J.H., A.Z., C.C.-R., L.H., B.B., and J.T.L. designed research; A.J.H., A.Z., L.H., and B.B. performed research; A.J.H., A.Z., C.C.-R., L.H., B.B., and J.T.L. analyzed data; and J.T.L. wrote the paper.

Reviewers: V.G.C., Howard Hughes Medical Institute/University of Michigan; and K.Y.S., Los Alamos National Laboratory.

Competing interest statement: J.T.L. is a scientific cofounder of Translate Bio and Fulcrum Therapeutics, and also serves as an Adviser to Skyhawk Therapeutics.

Published under the PNAS license.

Data deposition: The datasets for short RNA-seq reported in this paper have been deposited in the Gene Expression Omnibus (GEO) database, https://www.ncbi.nlm.nih.gov/geo (accession no. GSE139931).

[1]A.J.H., A.Z., and C.C.-R. contributed equally to this work.

[2]Present address: Southern Alberta Genome Sciences Centre, Department of Chemistry and Biochemistry, University of Lethbridge, Lethbridge, AB T1K6T5, Canada.

[3]Present address: Lab Central, Cambridge, MA 02139.

[4]To whom correspondence may be addressed. Email: lee@molbio.mgh.harvard.edu.

First published December 23, 2019.

Downloaded at UNIVERSITY OF MASSACHUSETTS on January 9, 2020

advancement of POL-II and in this way, affects promoter-proximal pausing of POL-II to retard transcription elongation (23). On stress, the chromatin binding pattern shifts globally and dramatically. The Polycomb protein, EZH2, is rapidly recruited to heat shock genes and triggers cleavage of B2 RNA within 15 min of heat shock. Intriguingly, B2 cleavage is site specific (Fig. 1*B*). Turnover of B2 then relieves the transcriptional block and enables up-regulation of stress-inducible genes. Thus, EZH2 and B2 together control activation of a large network of genes involved in thermal stress.

These recent findings raise important questions regarding the cleavage mechanism. While EZH2 is well known for its methyltransferase activity that trimethylates histone H3 at lysine 27 (24) and is also well established as an RNA-binding protein (25–32), the protein lacks any recognizable ribonuclease (RNase) domain and was not previously known to have any nuclease activity. Yet, in a purified 2-component system, incubation of EZH2 with B2 RNA consistently results in site-specific cleavage, whereas exposure of EZH2 to other RNA species does not result in RNA turnover (23). Here, we investigate how EZH2 triggers B2 cleavage. To our surprise, we find that B2 is a self-cleaving RNA that depends on EZH2 to accelerate its intrinsic activity. We propose that B2 SINE is an epigenetic ribozyme that functions as a transcriptional switch during the stress response.

Results

B2 Cleavage Does Not Require the Histone Methyltransferase (HMTase) Activity of EZH2. Given that EZH2 lacks any recognizable RNase sequence motifs and does not exhibit cleavage activity when incubated with other tested RNA (23), we hypothesized that B2 cleavage may be an intrinsic property of the RNA. In this case, EZH2's established catalytic function (HMTase) would likely not be required. We examined EZH2–B2 interactions in the presence of 2 EZH2 inhibitors, PF-06821497 (PF) and tazemetosta (Taz), at concentrations above their IC_{50} (11 to 16 nM). Treatment with 30 or 300 nM PF or Taz did not block RNA processing (Fig. 1*C*). However, replacing EZH2 with another PRC2 subunit, EED, inhibited RNA processing. Thus, EZH2's catalytic activity is not required for B2 turnover.

B2 Is a Native Self-Cleaving RNA. We, therefore, turned attention to intrinsic properties of B2 RNA. Because B2 RNA cleavage occurred at an almost negligible rate in the absence of protein (Fig. 1*D*, lane 2), we surmised that EZH2's role may be to passively promote a B2 conformation that activates the self-cleavage reaction. In this case, experimental conditions might be found that would recapitulate cleavage competence in the absence of protein. The observed protein cofactor dependence of B2 cleavage was reminiscent of the requirement of protein chaperones for self-splicing of Group II introns (33). Because certain Group II introns can autoreact in the absence of protein under high salt concentrations, we tested published protein-free conditions for Group II intron (34). We first confirmed that the 180-nt B2 RNA in 10 mM Tris, pH 7.5, and 1 mM ethylenediaminetetraacetic acid (EDTA) was stable in vitro for >30 min to hours when incubated without EZH2 protein and $MgCl_2$, with no cleavage observed even at longer incubations (Fig. 1*D*, lane 1) (23). We furthermore confirmed that the presence of purified recombinant EZH2 and $MgCl_2$ triggered rapid RNA cleavage (Fig. 1*D*, lane 2) (23). To determine if high salt would recapitulate the activity in the absence of EZH2, we varied the monovalent cation (KCl vs. NH_4Cl) and tested it under low (100 mM) vs. high (500 mM) concentrations. We also varied the concentration of $MgCl_2$ (10 vs. 100 mM), a divalent cation known to be required for ribozyme activity. However, none of the high-salt protein-free conditions resulted in obvious B2 RNA cleavage after 30 min, regardless of whether KCl or NH_4Cl was used as monovalent cation (Fig. 1*D*). Thus, B2 RNA was generally unreactive in high-ionic strength conditions typically used for Group II intron reactions.

Interestingly, however, we observed that B2 could initiate cleavage on its own under the specific physiological concentrations of $MgCl_2$ (10 mM) and KCl (100 mM), albeit at reduced efficiency (Fig. 1*D*, lane 3). The cleavage pattern appeared similar between the 2 conditions, resulting in a number of shorter products as shown previously (Fig. 1*D*) (23). To rule out contamination by a nuclease, we pretreated the reaction with proteinase K before addition of B2 RNA. RNA cleavage still occurred after 1 h of incubation under a variety of physiological salt conditions (Fig. 1*E*), including TAP100 (lane 2: 100 mM NaCl, 50 mM Tris·HCl, pH 7.9, 0.11% Nonidet P-40, 0.2 mM EDTA, 5 mM $MgCl_2$, 2 mM dithiothreitol [DTT], 15% glycerol) and HMK (25 mM Hepes, pH 7.5, 100 mM KCl, 10 mM $MgCl_2$; lane 3). RNA cleavage was observed with either Na^+ or K^+ as monovalent cation. Notably, with or without proteinase K treatment, the reaction proceeded similarly after 1 h (Fig. 1*E*), indicating that protein is not required for cleavage. However, addition of EZH2 accelerated the reaction considerably, resulting in end products after 30 min of incubation (Fig. 1*F*).

Importantly, the effect of EZH2 was specific to B2 RNA as incubation of EZH2 with the high-affinity ligand, RepA (29), or any other RNA (23) did not result in any noticeable cleavage after 1 h (Fig. 1*G*). We also noted that a B2 variant used previously, here designated B2-J (20), showed weak self-cleaving activity and was more dependent on EZH2 for cleavage (Fig. 1*G*, lanes 5 and 6), thereby providing further evidence for dependence of cleavage activity on specific RNA species. B2-J differed by 1) an additional G at the 5′ end, 2) A → C change at nt 55, and 3) T → C change at nt 114, suggesting that sequences around these bases may be important for cleavage. Together, these findings provide an indication that B2 has self-cleaving activity. We propose that B2 is a self-cleaving ribozyme.

B2 Self-Cleavage Is Accelerated >100-Fold by Presence of EZH2. Our data indicate that the presence of EZH2 enhances B2's intrinsic activity. To test additional conditions that promote self-cutting, we asked if addition of the cationic peptide, protamine sulfate, could also recapitulate self-cleavage under physiological concentrations of monovalent and divalent cations. Indeed, addition of protamine sulfate without EZH2 also led to initiation of RNA cleavage (Fig. 2*A*). To calculate the cleavage rate, we preincubated B2 or control RepA RNA in HMK buffer, split the reaction in 2, and then added either protamine sulfate or EZH2 to stimulate the reaction (Fig. 2 *A* and *B*). Time course analysis showed that both the rate and the extent of B2 cleavage were greater in the presence of EZH2 relative to protamine sulfate, with the former reaching saturation within 3 min at 37 °C and the latter being still considerably under it (Fig. 2*C*). With EZH2, nearly 90% B2 reacted after 20 min at 37 °C, whereas only 20% reacted with protamine sulfate. Nonlinear fitting of the fraction of B2 RNA cleaved as a function of time to a single-exponential rate equation provided values for the observed cleavage rate constant, k_{obs}, which were 1.3 min^{-1} in the presence of EZH2 and 0.01 min^{-1} in the presence of protamine sulfate (Fig. 2 *C* and *D*)—further supporting EZH2's role in accelerating the cleavage reaction. Notably, because of our optimized conditions, these values are higher than our previously reported values (23) and indicate a more efficient in vitro reaction. Specifically, addition of protamine sulfate led to higher cleavage activity without protein. Moreover, a lower ionic strength likely facilitated the binding of EZH2 to B2 RNA, thereby further stimulating the cleavage rate. These findings were specific to B2 as the control RepA RNA did not exhibit EZH2- or time-dependent cleavage (Fig. 2 *B–D*). Thus, B2 can catalyze the cleavage reaction without assistance, but the presence of EZH2 accelerates the reaction rate by >100-fold. These data support the notion that B2 may be classified as a distinct type of self-cleaving ribozyme with a dependence on EZH2 to enhance its catalytic rate.

Downloaded at UNIVERSITY OF MASSACHUSETTS on January 9, 2020

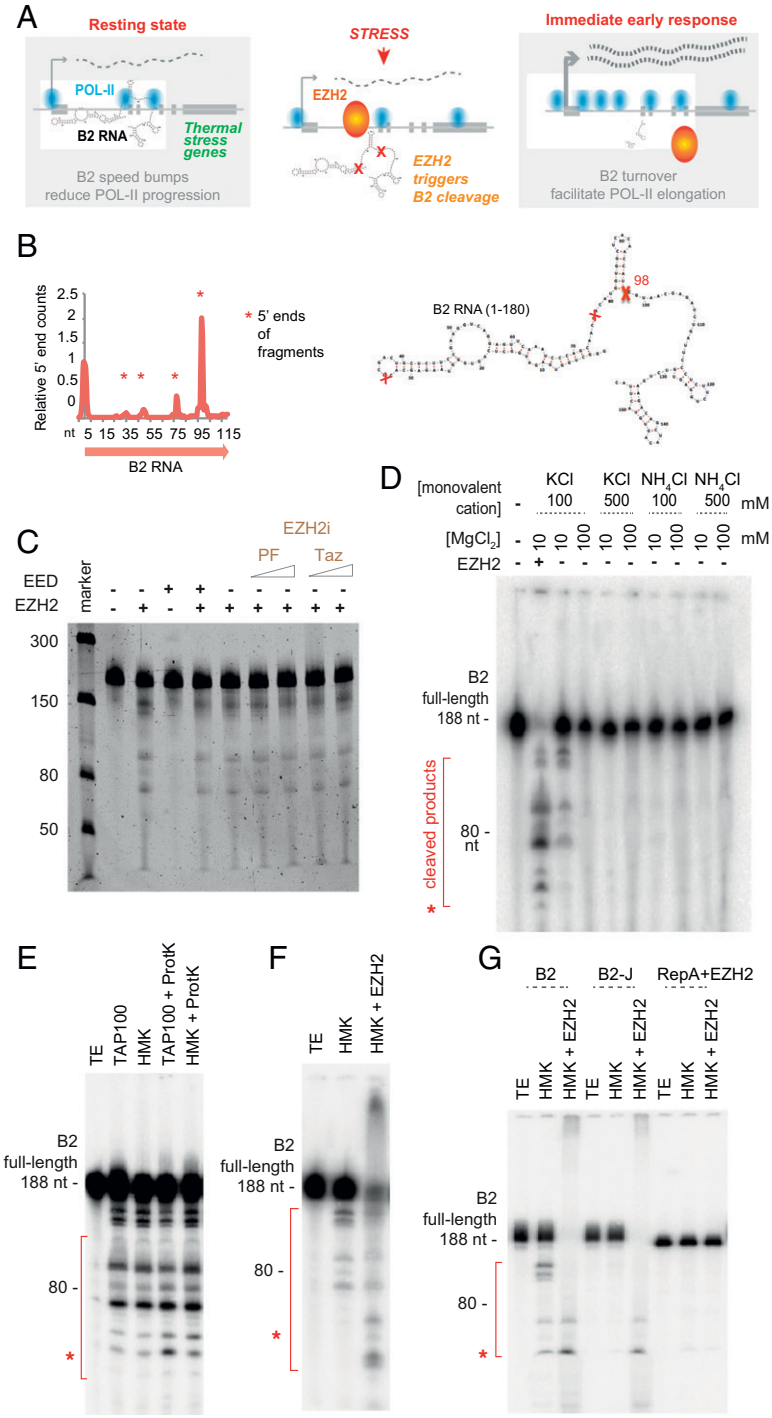

Fig. 1. Properties of EZH2-mediated B2 cleavage. (*A*) The B2 speed bump model adapted from ref. 23. In resting cells, B2 RNA binds stress-responsive genes and reduces their expression by forming speed bumps against POL-II elongation. When heat shocked, EZH2 is recruited and triggers B2 degradation. After the speed bumps are removed, the paused POL-II progresses through elongation, and the stress-inducible gene is expressed to combat heat shock. The speed bump mechanism enables a rapid and specific response to cellular stress. Changes are observed within 15 min of heat shock. Illustrations are adapted from ref. 23. (*B*) The 5′ cut sites of B2 RNA shown in the metagene (asterisks; *Left*) and RNA map (red X's; *Right*) as determined previously by short RNA-seq (23). Schematics are adapted from ref. 23. (*C*) EZH2's catalytic activity is not required for B2 processing; 200 nM B2 RNA was incubated with 25 nM EZH2 or EED, as indicated, for 40 min at 37 °C. Two catalytic inhibitors of EZH2, PF and Taz, were tested at 30 and 300 nM (IC_{50} 11 to 16 nM). (*D*) The 10 nM 5′ end-labeled full-length B2 RNA was incubated at 37 °C for 30 min in 10 mM Tris, pH 7.5; 1 mM EDTA (leftmost lane); or 25 mM Hepes-KOH, pH 7.5, supplemented with the indicated concentrations of KCl or NH_4Cl and $MgCl_2$. In lane 2, 0.5 μM purified recombinant EZH2 was added. Full-length B2 (180 nt) and cleaved products are indicated. (*E*) The 100 nM 5′ end-labeled B2 RNA was incubated at 37 °C for 1 h. Lane 1: TE; lane 2: TAP100 buffer (100 mM NaCl, 50 mM Tris·HCl, pH 7.9, 0.11% Nonidet P-40, 0.2 mM EDTA, 5 mM $MgCl_2$, 2 mM DTT, 15% glycerol); lane 3: HMK buffer; lane 4: TAP buffer pretreated with 10 μM proteinase K; lane 5: HMK buffer pretreated with proteinase K. *Cleaved B2 RNA. (*F*) The 100 nM 5′ end-labeled B2 RNA was incubated at 37 °C for 30 min in (lane 1) TE, (lane 2) HMK, or (lane 3) HMK plus 0.5 μM EZH2. *Cleaved B2 RNA. (*G*) EZH2 promotes cleavage of B2 RNA but not of RepA. Lanes 1 to 3: B2 RNA incubated in (lane 1) TE, (lane 2) HMK, or (lane 3) HMK + 0.5 μM EZH2; lanes 4 and 5: EZH2 + B2-J RNA incubated in (lane 4) TE or (lane 5) HMK; lane 6: HMK + 0.5 μM EZH2; lanes 7 to 9: RepA RNA incubated in (lane 7) TE, (lane 8) HMK, or (lane 9) HMK + 0.5 μM EZH2. RNAs were present at 10 nM and incubated as in *B*. *Cleaved B2 RNA.

Downloaded at UNIVERSITY OF MASSACHUSETTS on January 9, 2020

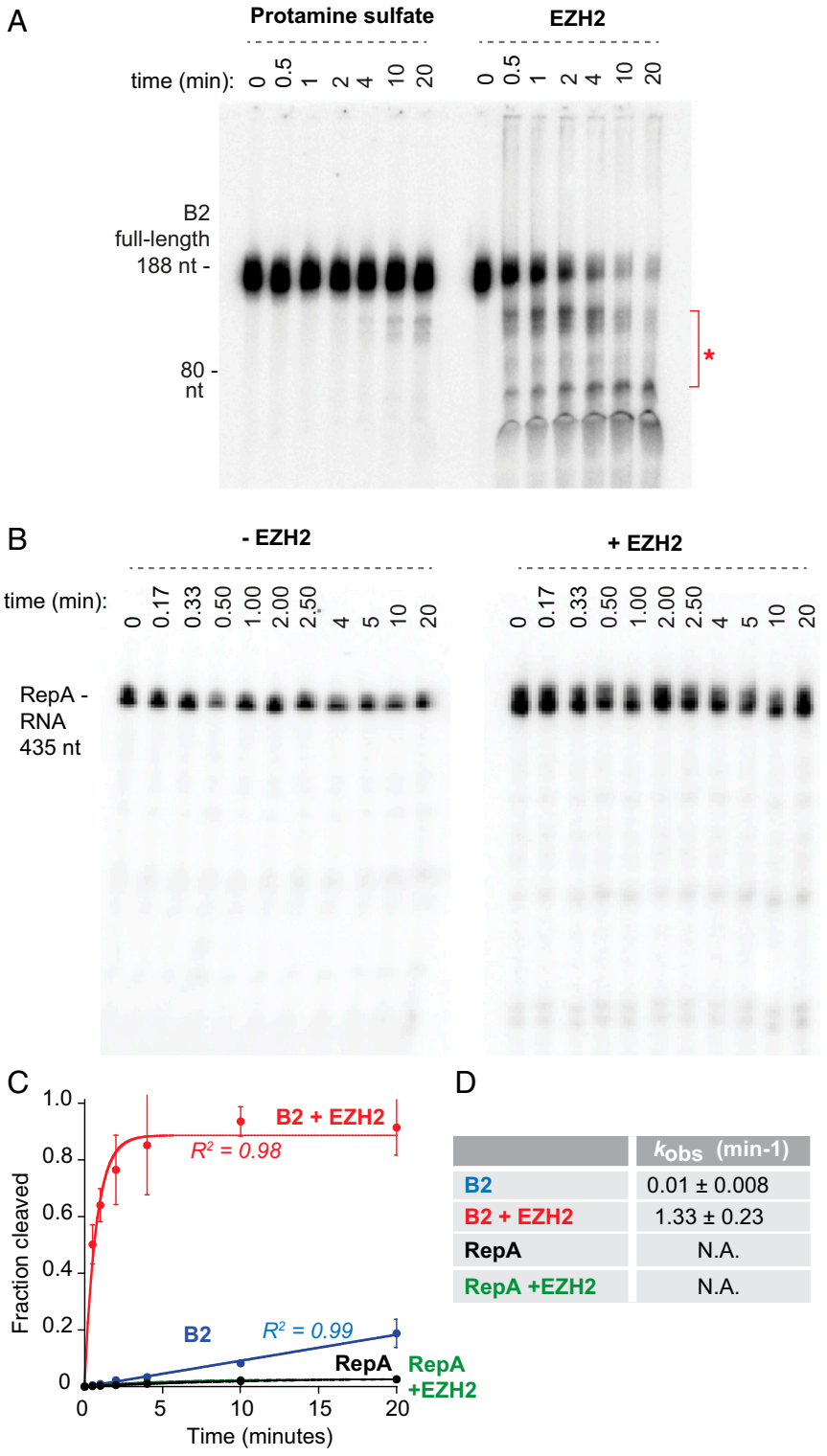

	k_{obs} (min-1)
B2	0.01 ± 0.008
B2 + EZH2	1.33 ± 0.23
RepA	N.A.
RepA +EZH2	N.A.

Fig. 2. EZH2 enhances the rate of B2 self-cleavage. (*A*) Time course of B2 RNA cleavage in the presence of protamine sulfate or EZH2; 10 nM internally labeled B2 RNA was incubated in HMK buffer at 37 °C for 20 min. Reactions were started with the addition of either 5 nM protamine sulfate or 500 nM EZH2. Aliquots were removed at 0, 0.5, 1, 2, 4, 10, and 20 min and quenched with formamide dye and dry ice. Shown are denaturing gels of the cleavage time course. *Cleaved B2 RNA. (*B*) Time course of RepA RNA stability with or without EZH2; 10 nM internally labeled RNA was incubated in HMK buffer at 37 °C for 20 min. Reactions were started with the addition of either 5 nM protamine sulfate or 500 nM EZH2. Aliquots were removed at 0, 0.5, 1, 2, 2.5, 4, 5, 10, and 20 min and quenched with formamide dye and dry ice. Shown are denaturing gels. (*C*) Plot of B2 or RepA RNA cleavage as a function of time. Error bars represent SDs from 3 independent experiments. (*D*) Accompanying table of k_{obs} values for *B*. Values for RepA ± EZH2 were too small to calculate accurately (not applicable [N.A.]).

Downloaded at UNIVERSITY OF MASSACHUSETTS on January 9, 2020

pH Dependence and Sensitivity to Chemical and Sequence Modifications. Protein cofactors for ribozyme activity are generally thought to operate by stabilizing a catalytically active conformation of the RNA. RNA can in principle fold into many possible conformations, a number of which might have equal stability, especially under high cation concentration. In vivo, however, interacting proteins can substitute for high ionic strength by stabilizing RNA conformations in part through steric constraint. Without protein partners, ribozymes generally show exquisite pH dependence and sensitivity to base modifications due to potential base arrangements and electrostatic changes around their cleavage sites (35). Accordingly, we observed that B2 cleavage also showed an exquisite pH dependence, with unassisted cleavage displaying a bell-shaped pH profile and an optimal activity at pH 6.5 to 7 (Fig. 3 *A* and *B*). This pH dependence suggests the presence of at least 2 ionizable groups involved in self-cleavage. In the presence of EZH2, however, B2 cleavage continuously improved into the basic range up to pH 9.0. Mitigation of pH sensitivity suggests that a residue in EZH2—most likely a basic, positive-charged residue—can substitute for the function of the ionizable group with the greater pKA in B2. This result supports a "chaperone" function for EZH2.

To probe further, we changed the phosphodiester (PO) backbone of specific B2 bases to phosphorothioates (PSs) (Fig. 3*C*)—a "modification-interference analysis" that has been used to probe for ribozyme activity (36, 37) as PS substitutions could potentially cause weaker binding to magnesium ions and stronger binding to "soft" metals (i.e., manganese), alteration of RNA folding by changing the charge distribution of the backbone and hydrogen bonds around modified groups, and steric effects owing to the greater atomic radius of sulfur relative to oxygen (38–40). For B2 RNA, PS substitutions for A and C phosphates did not inhibit cleavage. In fact, we observed a significant increase in cleavage activity, even in the absence of EZH2. Thus, PS substitutions at A and C can mimic the chaperone function of EZH2 and render B2 less dependent on EZH2 for cleavage. Introduction of PS sat G residues, however, inhibited B2 cleavage, arguing against a nonspecific effect of PS substitutions and suggesting that G phosphates may bind critical metal ions or EZH2 to establish an RNA conformation that is cleavage competent.

We also tested sequence variants of B2 RNA (Fig. 3 *D*–*F*); 5′ and 3′ truncations altered fragment sizes and number (Fig. 3*D*) as expected. Mutating 2 nt (nt 100 to 101) adjacent to the previously identified major cleavage site (nt 98 [23]) resulted in loss of cleavage product X and appearance of a much smaller fragment Y (Fig. 3*E*). This finding indicates that sequences around the central cleavage site are important for B2 activity in the presence of EZH2. While deleting 10 bases around nt 45 to 55 also altered the

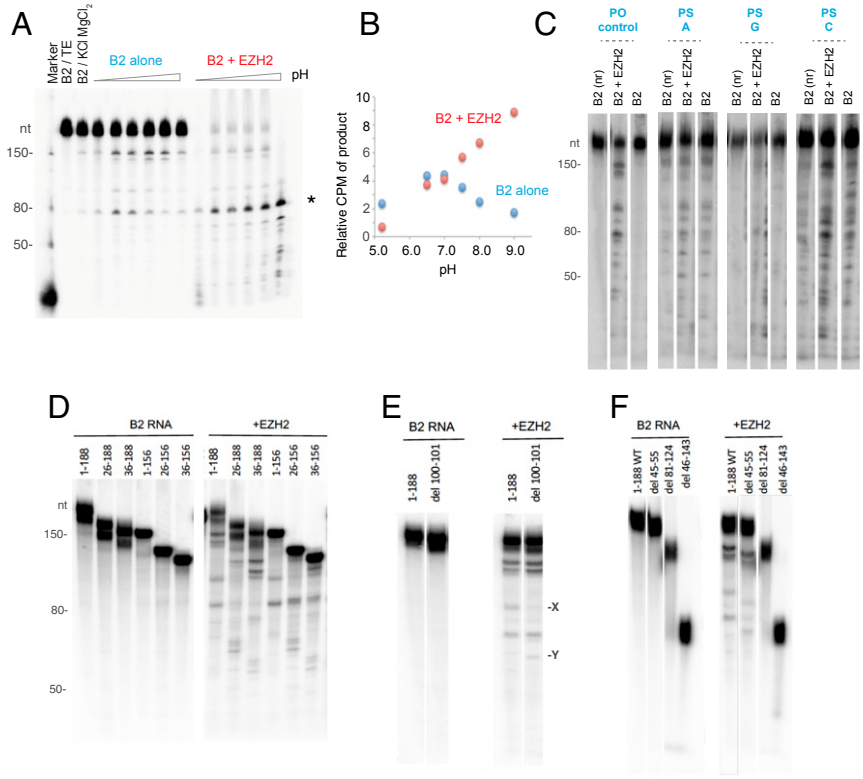

Fig. 3. Cleavage activity is affected by site-specific mutations and PS modification. (*A*) pH dependence of B2's cleavage reaction. Cleavage reaction of internally labeled B2 (10 nM) alone or in the presence of 500 nM EZH2 at 37 °C. RNA-only reactions were allowed to proceed for 45 min. RNA + EZH2 reactions were allowed to proceed for 5 min. Lane 2: B2 + TE (no reaction); lane 3: B2 + KCl + $MgCl_2$ (self-cleavage); lanes 4 to 9: B2 self-cleavage in increasing pH; lanes 10 to 15: B2 + EZH2 in increasing pH. *Cleavage product measured in *Lower*; relative counts per minute (CPM) of cleavage product (shown in *Upper*) plotted as a function of pH. (*B*) Quantitation of the experiment in *A*. (*C*) B2 cleavage with or without EZH2 after RNA is modified by base-specific PS substitutions as indicated. PS-A indicates that all A's in B2 are changed to a PS backbone. Control with PO backbone is shown. For each series, lane 1 shows B2 + TE (no reaction [nr]), lane 2 shows B2 + EZH2 under reaction conditions (KCl + $MgCl_2$), and lane 3 shows B2 alone under reaction conditions. (*D*) The 5′ and 3′ truncations of B2 affect EZH2-mediated cleavage. Lanes 1 to 7: RNA only and no reaction. Lane 1: Wild-type (WT) B2 (nt 1 to 188); lane 2: B2 nt 26 to 188; lane 3: B2 nt 36 to 188; lane 4: B2 nt 1 to 156; lane 5: B2 nt 26 to 156; lane 6: B2 nt 36 to 156. Lanes 7 to 12: RNA cleavage reactions in HMK buffer + 0.5 μM EZH2 at 37 °C for 10 min. Lane 7: WT B2 (nt 1 to 188); lane 8: B2 nt 26 to 188; lane 9: B2 nt 36 to 188; lane 10: B2 nt 1 to 156; lane 11: B2 nt 26 to 156; lane 12: B2 nt 36 to 156. (*E*) Nt 100 to 101 is essential for proper cleavage pattern. (*F*) Deleting nt 45 to 55 partially affects activity, while deleting nt 81 to 124 or 46 to 143 abrogates all cleavage activity. Lane 1: WT B2 (nt 1 to 188); lane 2: del 45 to 55; lane 3: del 81 to 124; lane 4: del 46 to 143.

Downloaded at UNIVERSITY OF MASSACHUSETTS on January 9, 2020

cleavage pattern, deleting either nt 81 to 124 or 46 to 145 resulted in a complete loss of all cleavage activity (Fig. 3*F*). These data identify sequences around the major cleavage site and nt 45 to 55 as essential. The fact that mutating specific nucleotides can affect cleavage in the presence of EZH2 further argues that cleavage activity is an intrinsic property of B2.

Human ALU RNA Also Self-Cleaves in an EZH2-Dependent Manner. In humans, the most abundant SINE is the ALU, named for the *Alu-I* restriction site occurring in these elements. ALUs belong to the B1 family of SINEs and are divided further into 3 subfamilies—ALU J, ALU S, and ALU Y, each being dimeric in structure and ~300 nt in length (9, 41) (Fig. 4*A*). Like murine B2, human ALUs are transcribed by POL-III, are most highly expressed during early development, and become epigenetically unsilenced during cellular stress (11–13). ALUs have also been implicated in the heat shock response in human cells (42).

Given the phylogenetic and epigenetic similarities, we wondered if ALU RNA is also cleaved. We derived consensus sequences for the 3 ALU subfamilies J, S, and Y (9) and examined their behavior in the presence of purified EZH2. Intriguingly, all 3 ALU sequences appeared to self-cleave to varying extents. Indeed, whereas all 3 ALUs remained stable when incubated in Tris-EDTA buffer (TE) for 10 min at 37 °C, they began to autoreact and generate smaller products when incubated in HMK buffer, the same buffer that revealed ribozyme-like properties in B2 (Fig. 1). As for B2 RNA, the ALU reaction was enhanced in the presence of EZH2 in HMK buffer (Fig. 4*B*, lane 3 in each subfamily). In contrast to B2, cleavage of ALU RNAs was not significantly stimulated by addition of protamine sulfate, suggesting that the folding pathway leading to a cleavage-competent conformation may be less energetically steep for ALUs than for B2. This is consistent with the observation that ALU self-cleavage is more readily detected even after a short incubation period (10 min.).

We then measured the rate of ALU self-cleavage. Interestingly, ~40% of ALU RNA underwent self-cleavage within 5 min (Fig. 5*A*). We determined the observed rate constants for the initial cleavage step by nonlinear fits of the fraction of RNA cleaved as a function of time to a rate equation (Fig. 5 *B–D*). In the absence of EZH2, ALU subfamily types showed slight differences in the rate of cleavage. The rate of cleavage of ALU J was about twice that of ALU S, which was in turn twice as fast as ALU Y. We note that the rates of self-cleavage are inversely proportional to their genomic insertion activities: ALU Y is more active followed by ALU S and finally, by ALU J (9). In general, the reaction proceeded with faster kinetics for all 3 ALUs than for B2s (Fig. 2). Indeed, even without EZH2, ALU J exhibited a nearly 40-fold higher rate (k_{obs}) than B2.

When incubated with EZH2, the observed rates were increased for all 3 ALU subfamilies (Fig. 5 *B–D*). Without EZH2, ALU J had the highest k_{obs} of 0.37 min^{-1}, and EZH2 accelerated the cleavage rate by 6-fold. The rate for ALU S increased 4-fold from 0.37 to 2.1 min^{-1}. Additionally, that for ALU Y increased 33-fold from 0.06 to 1.98 min^{-1}. Approximately 70 to 80% of all 3 RNAs was cleaved, with a k_{obs} of ~2 min^{-1}. Interestingly, when assisted by EZH2, the rate and extent of cleavage of all 3 ALU RNAs were nearly identical. Thus, while all ALU RNA subfamilies—to varying degrees—have the intrinsic capacity to fold efficiently into a cleavage-competent conformation, contact with EZH2 greatly accelerates this folding transition. We conclude that ALUs and B2s both can self-cleave, but ALUs have higher intrinsic activity. EZH2 functions as a cofactor for both ribozymes.

Human ALU RNA Is Up-Regulated and Cleaved during Stress and T-Cell Activation. We previously established B2 as a crucial regulator of the thermal stress response in mouse cell (23). To investigate whether ALU RNA is also cleaved under stress conditions in humans, we performed northern blot analysis of ALU RNA in human T cells before and after heat shock. ALU RNA was not only up-regulated as expected (42) but also cleaved as evidenced

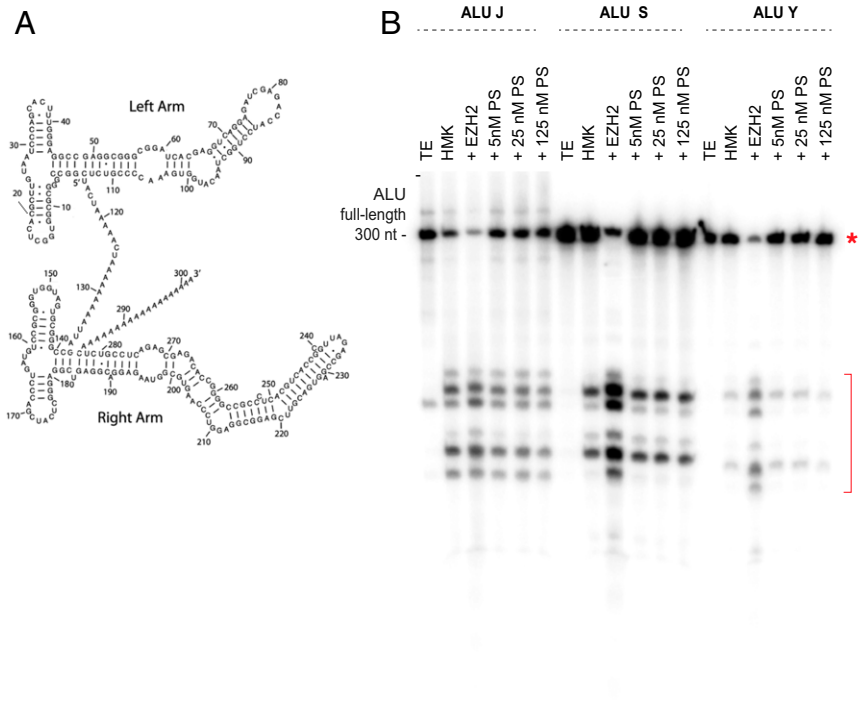

Fig. 4. EZH2 enhances cleavage of ALU RNAs in vitro. (*A*) Human ALU consensus sequence and secondary structure adapted from Hadjiargyrou and Delihas (41). ALU sequence consists of a sequence dimer, of which the monomers constitute its left and right arms. (*B*) The 100 nM internally labeled ALU J, S, and Y RNAs were incubated at 37 °C for 10 min in (lane 1) TE, (lane 2) HMK buffer, (lane 3) HMK plus 0.5 μM EZH2, (lane 4) HMK plus 5 nM protamine sulfate, (lane 5) HMK plus 25 nM protamine sulfate, and (lane 6) HMK plus 125 nM protamine sulfate. The RNAs are indicated above. PS, protamine sulfate.

Downloaded at UNIVERSITY OF MASSACHUSETTS on January 9, 2020

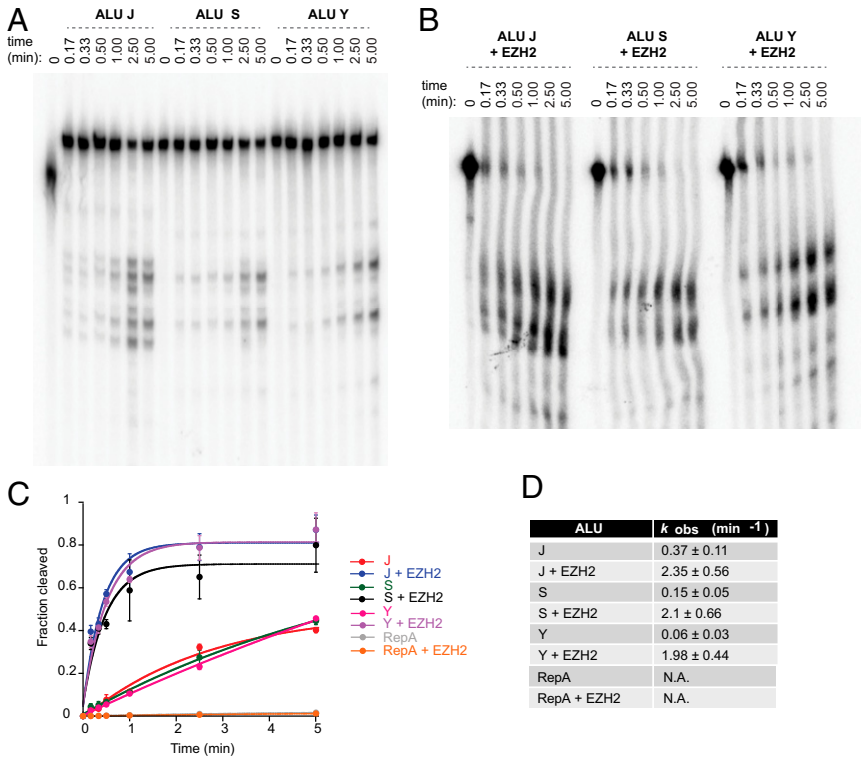

ALU	k_{obs} (min $^{-1}$)
J	0.37 ± 0.11
J + EZH2	2.35 ± 0.56
S	0.15 ± 0.05
S + EZH2	2.1 ± 0.66
Y	0.06 ± 0.03
Y + EZH2	1.98 ± 0.44
RepA	N.A.
RepA + EZH2	N.A.

Fig. 5. ALU self-cleavage is stimulated by EZH2. (*A*) Time course of ALU RNA cleavage in the presence of protamine sulfate; 10 nM internally labeled RNA was incubated in HMK buffer at 37 °C for 5 min. Reactions were started with the addition of 5 nM protamine sulfate. Aliquots were removed at 0, 0.17, 0.33, 0.5, 1, 2.5, and 5 min and quenched with formamide dye and dry ice. (*B*) Time course of ALU RNA cleavage in the presence of EZH2; 10 nM internally labeled RNA was incubated in HMK buffer at 37 °C for 5 min. Reactions were started with the addition 500 nM EZH2. Aliquots were removed at 0, 0.17, 0.33, 0.5, 1, 2.5, and 5 min and quenched with formamide dye and dry ice. (*C*) ALU RNA cleavage as a function of time in the absence or presence of EZH2. Error bars represent SDs from 3 independent experiments. (*D*) The observed cleavage rate constants from *C* are indicated in the table. R^2 values are 0.98, 0.96, 0.99, 0.93, 0.99, and 0.96 in the order shown in the key, indicating excellent fit of datapoints to the curve.

by the increase in smaller fragments in the northern blot after 15 min of heat shock (Fig. 6). (Note that higher-molecular weight bands at >1,000 nt correspond to ALU elements embedded within messenger RNA [mRNA] and introns.) To ask whether other types of stresses could induce ALU RNA and lead to its cleavage, we induced endoplasmic reticulum (ER) stress by subjecting human T cells to tunicamycin—an antibiotic that interferes with protein folding and causes dysfunction of ER in a manner that is known to activate ER stress (43, 44). We also subjected the T cells to PMA/Ionomycin—a drug mixture that also causes stress and triggers robust immune activation (45, 46). Both types of stress resulted in a striking up-regulation and cleavage of ALU as evidenced by the appearance of lower-molecular weight ALU RNA species in the northern blot (Fig. 6). However,

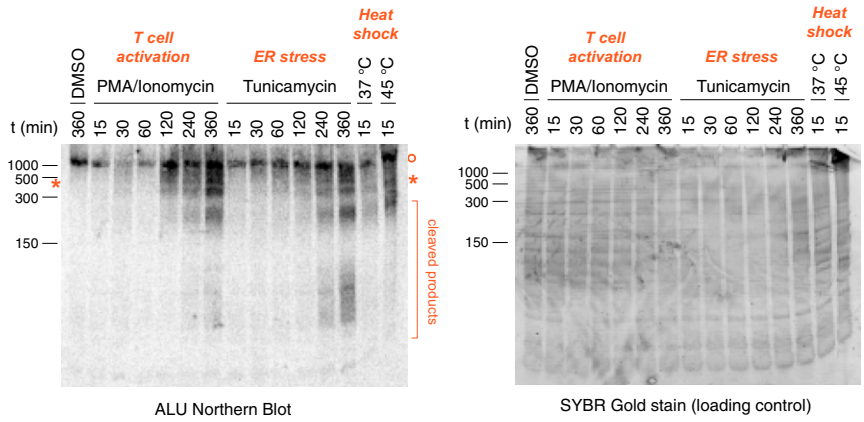

Fig. 6. Human ALU is up-regulated and cleaved during thermal and ER stress as well as T-cell activation. ALU is up-regulated and cleaved during T-cell activation and ER stress as well as thermal stress. Immortalized human T cells (Jurkat) were exposed to dimethylsulfoxide (DMSO) (control), 80 ng/mL PMA and 1 μM Ionomycin mixture (T-cell activator), 10 μg/mL tunicamycin (ER stress inducer), or 45 °C (heat shock) for indicated time periods. Northern blot was performed to detect Alu RNA species in total RNA isolates. SYBR Gold staining is used as loading control. Cleaved ALU is as indicated. The orange circle indicates ALU embedded in mRNA and introns. *Full-length ALU.

Downloaded at UNIVERSITY OF MASSACHUSETTS on January 9, 2020

whereas ALU up-regulation and cleavage were observed within 15 min of thermal stress, they were observed over a longer timeframe, between 2 and 6 h, in the case of ER stress and T-cell activation. Thus, ALU cleavage is not restricted to thermal stress but can be generalized to at least 2 other types of stresses.

In Vivo Analysis of ALU Cut Sites. We next wished to determine the cut site within human ALU RNA. In HeLa cells, we performed short RNA sequencing (RNA-seq), a protocol that enriches for native transcripts in the 40- to 300-nt size range (23), and mapped the short RNA-seq reads against an ALU consensus metagene derived from mm9 genomic ALU elements. We then aligned the 5′-end start points of all ALU fragments to the 300-nt consensus and observed a strong peak at positions 49 to 52 of the left arm. This peak suggested a discontinuity or cleavage at nt 49 to 52. Because each ALU element can have a number of variations from the consensus sequence, the cut position varies according to the insertions and deletions present in each ALU. To reduce the number of sequence variations, we repeated the alignment using only reads from the ALU Y subfamily and observed a sharp peak at nt 51 (Fig. 7*A*). Notably, a similar cut might also occur in the right arm of the ALU dimer. Because the 2 arms are highly homologous, it is not possible to distinguish cuts in the 2 arms through sequence alignment. However, based on the sizes of the in vitro cleavage profiles (Fig. 5), we suggest that both ALU arms are cleaved. Taken together, these data indicate that ALU is also a native self-cleaving RNA. Although ALUs also depend on EZH2 for kinetic enhancement, ALUs are intrinsically more autoreactive than B2 RNA, with ALU J being most reactive.

Lastly, we compared the ALU J, S, and Y consensus sequences in the left arm to identify differences that might potentially explain why ALU J has greater intrinsic reactivity (Fig. 7*B*). Intriguingly, the existence in ALU J of a TG instead of a CA at positions 62 to 63 would likely destabilize a stem structure that is present in ALU Y, while the occurrence of a C (in ALU J) instead of U at position 69 would stabilize the stem structure (Fig. 7*C*). Along the same stem at position 92, the C is replaced by a G in ALU J, disturbing base pairing in the stem, while in position 99, the existence of an A in ALU J in combination with the existence of the extra Ts directly opposite between positions 64 and 65 and the lack of base pairing at 62 to 63 could shift the stem position 1 base to the right for ALU J, thereby enlarging the internal loop. Furthermore, ALU Y has a U instead of G at position 86, which would thereby elongate the stem, while at position 93, the lack of a C would destabilize this stem. Any of the above changes could have a dramatic impact on the secondary and tertiary structure of the ALU classes, potentially explaining the relative ease with which ALU J could adopt a cleavage-competent conformation, even in the absence of EZH2. Nucleotide changes in the right arm could similarly affect cleavage rates, either directly for cutting within the right arm or indirectly for cutting in the left arm through tertiary structures or allosteric interactions.

Discussion

Prior to the discovery of RNA catalysts called ribozymes, enzymatic proteins were the only known macromolecules capable of catalyzing biochemical reactions (47, 48). In the past 4 decades, ∼15 classes of ribozymes have been validated across various taxa, largely in bacteria and phages (33, 49–52). Ribozymes have also been predicted using comparative genomics (51) and chemically created in vitro using systematic evolution of ligands by exponential enrichment (53, 54). Well-established ribozymes include peptidyl transferase, which polymerizes amino acids to form proteins, RNase P, and Groups I and II introns. Among all known ribozymes, only 6 are self-cleaving. Although RNA catalysts have garnered the interest of the pharmaceutical industry for years (55), the physiological functions of most naturally occurring or predicted ribozymes are not known. In mammals, 3 ribozymes have been proposed, including 1) CPEB3 ribozyme (an intronic HDV-like ribozyme) (54), 2) a ribozyme embedded in the human β-globin pre-mRNA (56), and 3) a discontinuous element in the 3′ UTR of rodent *Clec2* (57). The functions of these mammalian ribozymes are not understood at present.

Here, we have shown that the B2 SINE retrotransposon is an epigenetic ribozyme that functions as transcriptional switch during cellular stress. B2 and ALU appear unique in several ways. First, there is no obvious sequence similarity to other ribozyme classes, including the newer Twister, Pistol, and Hatchet classes. Twister ribozymes have the fastest catalytic rates and generally do not depend on a protein partner. Pistol and Hatchet ribozymes are both self-cleaving, but there is no evident sequence similarity between B2/ALU and any other self-cleaving ribozymes. Pistol and Hatchet also do not require protein cofactors. As we do not currently know the mechanistic details of B2/ALU cleavage, mechanistic similarities cannot be ruled out. Irrespectively, B2 and ALU are unique in being members of a large retrotransposon family (SINEs).

Second, another unusual feature is that B2 and ALU activity is accelerated by an epigenetic factor, EZH2. No other ribozyme, to our knowledge, depends on EZH2 for activity. The determinants for cleavage activity and site selection, however, appear to reside solely within B2 and ALU and are not enhanced by base pairing within an ribonucleoprotein (RNP) as is typical for RNA splicing within the context of the spliceosome. Furthermore, while EZH2 accelerates the rate of cleavage, it does not impart cleavage specificity or change the distribution of products. The idea that specific RNA-binding proteins can stimulate ribozyme activity finds precedence in several well-established ribozymes. Bacterial RNase P, for example, catalyzes PO bond hydrolysis in transfer RNA (tRNA) precursors and comprises 1 obligatory 350- to 400-nt RNA that creates the active site and 1 120-amino acid protein that is required for RNA activity under physiological conditions (48, 58). Two other examples include the Group I and Group II introns, both of which are self-splicing RNAs with splicing activities that are enhanced by binding to specific protein factors (33, 47, 59). In all cases, the protein cofactor is thought to bind specifically to the RNA, stabilize its catalytically active conformation, and thereby, enhance its catalytic rate. Indeed, RNA polymers can typically fold into many alternative secondary and tertiary structures, some of which may be equally stable. High cation concentration generally stabilizes RNA conformations in vitro, but this is impossible in vivo. Interacting proteins can perform the task of stabilizing RNA conformations very effectively in vivo.

In the case of B2 and ALU, intrinsic nuclease activity depends on physiological salt (10 mM $MgCl_2$ and 100 mM KCl). This activity is resistant to protease treatment, but contact with EZH2 accelerates cleavage rate by 100-fold for B2 and 40-fold for ALU. All 3 subfamilies of human ALUs (J, S, and Y) possess this property. As with other ribozymes, B2 is exquisitely sensitive to pH. Its narrow optimal range of pH 6.5 to 7.0 can be broadened to pH 9.0 when EZH2 is present, suggesting that a residue in EZH2—possibly a basic, positively charged residue—can substitute for the function of the ionizable group with the greater pKA in B2. Through mutagenesis, we identified specific regions of B2 RNA (nt 45 to 55 and 100 to 101) that influence B2 activity in the presence of EZH2. Interestingly, B2 ribozyme activity can not only be inhibited but can also be enhanced by specific PS substitutions. Such effects of PS have been observed previously with the other ribozymes (36, 37). It is tempting to speculate how PS substitutions might affect B2 activity. Our work shows that Mg^{+2} is a required cation for the B2 cleavage activity. Mg^{+2} is the most common cation in RNA structure, and contact with RNA can occur in the 2′-OH group or the oxygen atoms of the PO backbone (37). Mg^{+2} could play several roles in the B2 ribozyme, the first being in the active site as a cofactor for catalysis, playing either a direct or indirect role in the covalent transformation. A second role relates to an ionic cloud around the RNA for negative charge neutralization of the backbone phosphoryl groups. Introducing a

Downloaded at UNIVERSITY OF MASSACHUSETTS on January 9, 2020

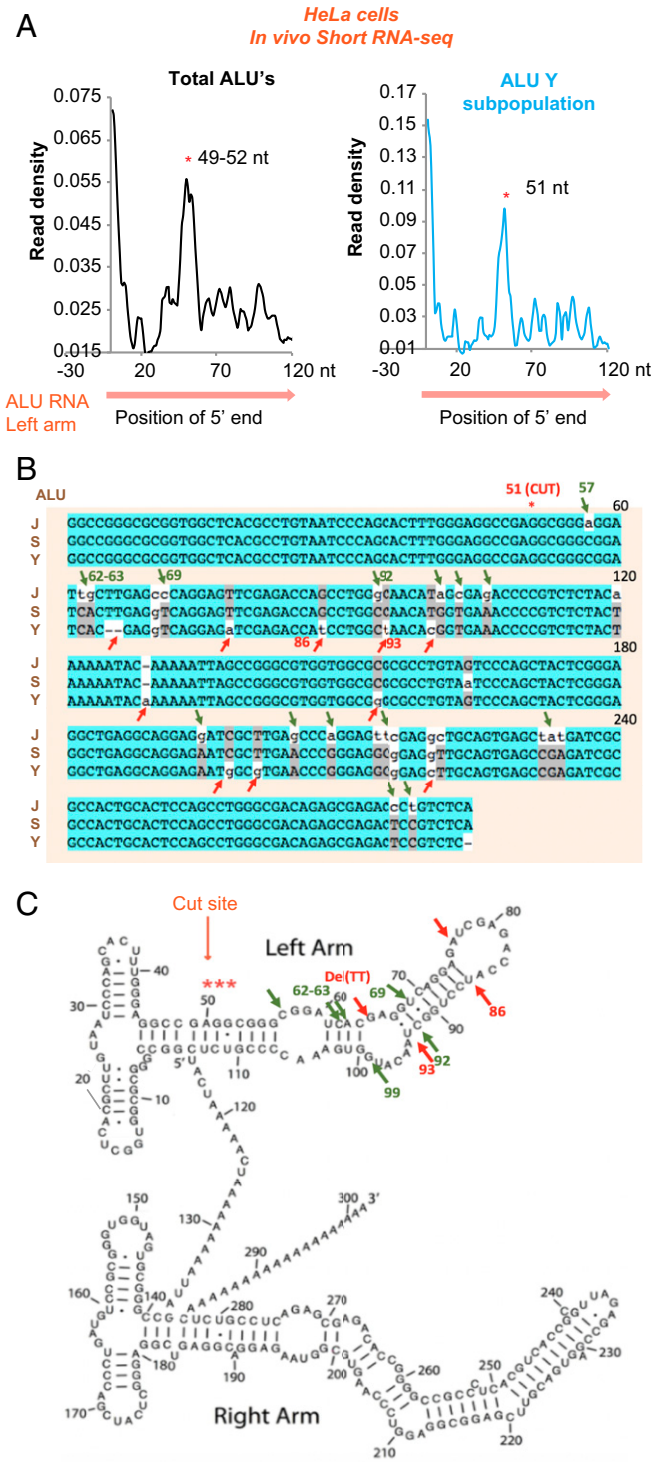

Fig. 7. In vivo analysis of ALU cut site. (*A*) Short RNA-seq of HeLa cells after 15-min heat shock at 45 °C. ALUs are cut at a position within the position range 49 to 52 from the start of the ALU SINE genomic elements. The graph shows 5′ ends of short RNA-seq reads mapped against mm9 genomic ALU elements creating the transcript metagene of the ALU elements. The metagene *x* axis is constructed by aligning the 5′ start points of all ALU RNAs as defined in UCSC repeat masker. The *x* axis position numbers represent absolute distance in nucleotides from the ALU start site (i.e., position 1 in the metagene corresponds to the start site of each ALU genomic element from which the ALU RNA transcript metagene is constructed). The relative number of short RNA 5′ ends is plotted on the *y* axis. Mapping is focused on only the first ALU arm (*Left*) to prevent cross-mapping because of sequence similarity between the 2 ALU sequence dimers. For a specific ALU class, ALU Y, the cut is at position 51. This is presented as an example of the cut point within a specific ALU subfamily. (*B*) Multiple alignments of the ALU J, S, and Y consensus sequences to compare sequence differences that potentially explain differences in intrinsic catalytic rate. Green arrows indicate ALU J differences relative to S and Y that could possibly explain its higher processivity. Red arrows indicate ALU Y differences that could potentially explain its lower processivity. *Cut site. (*C*) Sequence differences between ALU J and Y mapped onto the ALU Y structure proposed by Hadjiargyrou and Delihas (41). The color scheme is the same as that used in *B*. ***Cut sites.

thiophosphoryl group on the RNA backbone could, therefore, prevent Mg^{+2} binding. This change could affect the ribozyme both negatively and positively. A decrease in reactivity—as seen for PS substitutions at G's—could be due to perturbed metal ion binding or steric hindrance due to presence of a larger atom (sulfur vs. oxygen). An increase in reactivity—as seen for PS substitutions at A's and C's—could occur for the same reasons. Taken together, our data argue that EZH2 functions as a chaperone to fold B2 and ALU into a more favorable conformation for self-cleavage. Notably, this function of EZH2 does not depend on its canonical histone methyltransferase activity as pharmacologic inhibition of this activity does not affect its ability to stimulate B2 cleavage activity. Thus, our study also ascribes a distinct function to the classic epigenetic factor, EZH2.

Finally, given B2's interaction with EZH2 and a role in transcriptional modulation following thermal stress (Fig. 1*A*), B2 RNA could also be characterized as an "epigenetic ribozyme"—to our knowledge, the only ribozyme to date to play a role in epigenetic regulation. We surmise that ALUs may also be characterized as an epigenetic ribozyme. Indeed, our study together with recent work (23) links the ribozyme property of B2 and ALU RNAs to the stress response (Figs. 1 and 6). Cells are continually challenged by acute stress, and a swift response to environmental stress can mean the difference between life and death. Hinging the epigenetic induction of stress-related genes to turnover of these short RNAs seems highly adaptive because no new synthesis of gene products would be required, and the critical event would instead be the recruitment of a protein factor, EZH2, that already exists inside cells and stands ready to be mobilized. With B2 and ALU being present in hundreds of thousands of copies in mammals and being especially active in early development and during stress, their catalysis would likely represent the predominant ribozyme activity in mouse and human cells.

Materials and Methods

In Vitro RNA Cleavage. RNAs were transcribed in vitro with T7 RNA polymerase and purified by denaturing gel electrophoresis. RNAs were either internally labeled during transcription by using [α-^{32}P] nucleoside triphosphates (NTPs) or 5′ end labeled by treatment with alkaline phosphatase followed by incubation with T4 polynucleotide kinase and [γ-^{32}P] adenosine triphosphate (ATP). Labeled RNA in 10 mM Tris·HCl, pH 7.5, and 0.1 mM EDTA was incubated at 95 °C for 1 min followed by 5 min at 37 °C. Reactions were started by diluting heat-denatured RNA to a concentration of 10 nM in 25 mM Hepes-KOH, pH 7.5, 100 mM KCl, and 10 mM $MgCl_2$ in the presence of either 500 nM EZH2 or 5 nM protamine sulfate and incubated at 37 °C. For the analysis of fragment termini, RNAs were treated with either 2 U/μL ribonuclease R (Epicentre), 0.2 U/μL terminator nuclease (Epicentre), and 1 U/μL T4 polynucleotide kinase (PNK) (New England Biolabs) at 37 °C in the buffer supplied by the manufacturer or incubated with 25 mM sodium periodate in 60 mM borate buffer, pH 8.6, at room temperature for 30 min. Reactions were quenched with 2 volumes of formamide loading dye (93% formamide, 50 mM EDTA, 0.01% xylene cyanol, 0.01% bromophenol blue) followed by denaturing gel electrophoresis and phosphorimaging.

Time points for cleavage time courses were taken by manually withdrawing aliquots of the reaction mixture at the indicated times, quenched with 2 volumes of formamide loading dye, and immediately placed on crushed dry ice until all samples were collected. The fraction of cleaved RNA as a function of time was fit using Kaleidagraph (Synergy) to a single-exponential function: $y = A(1 - e^{-kt})$, where y is the fraction of cleaved RNA at a given time, A is the reaction amplitude, k is the observed rate constant, and t is time in minutes.

Downloaded at UNIVERSITY OF MASSACHUSETTS on January 9, 2020

RNA In Vitro Transcription and RNA–Protein Incubations. Proteins were prepared as previously described (29). Briefly, glutathione S-transferase (GST) was expressed in *Escherichia coli* BL21 transformed with pGEX4T1. Bacterial cell pellets were resuspended in lysis buffer (phosphate-buffered saline, 1% triton-X100, 1 mM DTT and protease inhibitors) and lysed by freeze-thawing followed by sonication. After centrifugation to remove cell debris, the extract was collected for purification by glutathione affinity chromatography. After binding to the beads, protein was eluted in 50 mM Tris8, 10 mM reduced glutathione, 1 mM DTT, and 0.1% Tween-20 and dialyzed in 10 mM Tris7.5, 100 mM NaCl, 5 mM $MgCl_2$, 0.1 mM $ZnSO_4$, 10% glycerol, and 0.1% Tween-20.

Mouse EZH2 and EED were expressed in Sf9 insect cells using the bac-to-bac system (Invitrogen). pFastBac1 expression vectors containing an N-terminal Flag-epitope–tagged EZH2 was obtained from the laboratory of Robert Kingston, Massachusetts General Hospital–Harvard Medical School, Boston, MA. Protein extracts were prepared by 3 freeze–thaw cycles in lysis buffer (50 mM Tris·HCl, pH 8.0, 300 mM NaCl, 1% Nonidet P-40, 0.3% Triton-X, 4 mM EDTA, 1 mM $MgCl_2$, 1 mM DTT, 20% glycerol, complete protease inhibitors [Roche]). M2 anti-Flag beads (Sigma) were used for all purifications. After binding and washes, proteins were eluted with 1-h incubations with 0.2 μg/mL 3×-Flag peptide (Sigma) and were concentrated using Amicon ultra concentrators (Millipore).

For RNA in vitro transcription, we used the AmpliScribe T7 High Yield Transcription Kit (Epicentre), applying a 3-h incubation at 42 °C and using a template resulting from the following B2 RNA sequence: 5′-GGGGCTGGTGAGATGGCTCAGTGGGTAAGAGCACCCGACTGCTCTTCCGAAGGTCCGGAGTTCAAATCCCAGCAACCACATGGTGGCTCACAACCATCCGTAACGAGATCTGACTCCCTCTTCTGGAGTGTCTGAAGACAGCTACAGTGTACTTACATATAATAAATAAATAAATCTTTAAAAAAAAA-3′. DNA template for the transcription was a PCR-amplified product derived from a gBlock (IDT) using as forward primer the T7 (5′-TAATACGACTCACTATAG) and as reverse primer for B2 RNA PCR template the following sequence: 5′-TTTTTTTTTAAAGATTTATTTATTTATTATATGTAAGTACA.

The ALU consensus sequences used for the in vitro transcription for the 3 subclasses are as follows.

"J," ALU Jo. The sequence is tggccgggcgcggtggctcacgcctgtaatcccagcactttgggaggccgaggcgggaggattgcttgagcccaggagttcgagaccagcctgggcaacatagcgagaccccgtctctacaaaaaatacaaaaattagccgggcgtggtggcgcgcgcctgtagtcccagctactcgggaggctgaggcaggaggatcgcttgagcccaggagttcgaggctgcagtgagctatgatcgcgccactgcactccagcctgggcgacagagcgagaccctgtctca.

"S," ALU Sz. The sequence is ggccgggcgcggtggctcacgcctgtaatcccagcactttgggaggccgaggcgggcggatcacttgaggtcaggagttcgagaccagcctggccaacatggtgaaaccccgtctctactaaaaatacaaaaattagccgggcgtggtggcgcgcgcctgtaatcccagctactcgggaggctgaggcaggagaatcgcttgaacccgggaggcggaggttgcagtgagccgagatcgcgccactgcactccagcctgggcgacagagcgagactccgtctca.

"Y," ALU Y. The sequence is ggccgggcgcggtggctcacgcctgtaatcccagcactttgggaggccgaggcgggcggatcacgaggtcaggagatcgagaccatcctggctaacacggtgaaaccccgtctctactaaaaatacaaaaaattagccgggcgtggtggcgggcgcctgtagtcccagctactcgggaggctgaggcaggagaatggcgtgaacccgggaggcggagcttgcagtgagccgagatcgcgccactgcactccagcctgggcgacagagcgagactccgtctca.

RepA sequence is as published (29).

RNAs were purified using the ZymoResearch RNA clean kit. Incubations, unless mentioned differently in the text, were performed with 200 nM in vitro-transcribed B2/ALU RNA folded with 300 mM NaCl and supplemented with TAP buffer (final reaction concentrations: 5 nM Tris, pH 7.9, 0.5 mM $MgCl_2$, 0.02 mM EDTA, 0.01% Nonidet P-40, 1% glycerol, 0.2 mM DTT). For RNA folding, the RNA was incubated for 1 min at 50 °C and cooled down with a rate of 1 °C/10 s. We monitored the disappearance of full-length B2 or ALU by denaturing polyacrylamide gel electrophoresis (PAGE) followed by SYBR Green II staining for 30 min. Cleavage time courses were quantified using ImageJ (NIH). The fraction of full-length RNA present at each time point was measured by taking the ratio of the size-corrected intensity of B2 or ALU RNA and dividing by the sum of size-corrected intensities for all gel bands. Cleavage data were fit using Kaleidagraph (Synergy) to the differential form of the rate equation for an irreversible, first-order reaction to derive an observed cleavage rate constant, k_{obs}.

Analysis of Human T-Cell Stress Response. Human immortalized T cells (Jurkat) were cultured in RPMI-1640, 10% fetal bovine serum (FBS), and 1% penicillin-streptomycin-neomycin (PSN). Jurkat cells were a gift from Brian Seed Laboratory, Department of Molecular Biology, Massachusetts General Hospital, Boston, MA. Ionomycin, calcium salt, *Streptomyces* conglobatus (catalog no. 407952) and PMA, phorbol-12-myristate-13-acetate (catalog no. 524400) were obtained from Calbiochem. Tunicamycin (catalog no. 654380–10MG) was obtained from Millipore Sigma. For northern blot analysis of ALU, total RNA was isolated according to the manufacturer's protocol using TRIZOL reagent (Life Technologies Corporation; catalog no. 15596–018); 7 μg RNA per lane was separated on 8 M urea/6% PAGE gel. RNA was transferred to N+ Hybond Nylon Membrane (GE Healthcare; catalog no. RPN303S). Hybridization was performed overnight at 58 °C with ^{32}P-labeled oligo probe directed against a universal ALU probe (sequence 5′–3′: GGTTTCACCGTGTTAGCCA). Following 3 × 15-min washes in 2× SSC and 0.1% SDS (Life Technologies Corporation; catalog no. 15557044) at 58 °C, membrane was exposed and analyzed.

In Vivo Analysis of ALU Cleavage Sites in Human Cells. In vivo analysis of cleavage sites was performed as in ref. 23 with slight modifications as follows. HeLa cells were cultured in Dulbecco's Modified Eagle Medium (DMEM) supplemented with Glutamax (Life Technologies) supplemented with 10% FBS and 1% penicillin/streptomycin. Before heat shock stimulus, cells were trypsinized and resuspended in 5 mL complete medium in a 15-mL falcon tube. Subsequently, cells were placed at 45 °C for 15 min. After the end of this 15-min period, cells were centrifuged shortly (2 min), and cell pellets were directly resuspended into TRIzol (Thermofischer) for the RNA-seq analysis. HeLa RNA used for short RNA-seq was prepared as follows. Total RNA from HeLa cells was extracted using TRIzol, and 4 μg of total RNA was subjected to ribosomal RNA depletion using the ribominus V2 kit (Life Technologies). Incubation of the RNA with the probe was done for 40 min instead of 20 min. RNA-depleted RNA was separated into 2 fractions of short (<300) and longer RNAs using the mirVana separation kit (Life Technologies) with the following modifications. After addition of the lysis/binding buffer and the microRNA (miRNA) homogenate additive solution, 100% EtOH at 1/3 of the volume was added, and the mix was passed through the filter to bind long RNAs. The flow through was collected, and 100% EtOH at 2/3 of the flow-through volume was added and passed through a new filter column to bind short RNAs. Elution of the long and short RNAs from each column was done per the manufacturer's instructions. Eluted RNAs were concentrated in both cases using the RNeasy MinElute Spin Columns (Qiagen) and tested for size and quality using an Agilent Bioanalyzer RNA kit. For short RNA library construction, ribo-depleted short RNAs were subjected to PNK 3′-phosphoryl removal for 1 h at 37 °C. Subsequently, we used the NEBnext small RNA library construction kit (NEB) with the following modifications. Incubation of the 3′ adaptor was performed for 2 h, and the libraries at the end were not subjected to double size selection with the Ampure beads but with 1.2× size selection. For sequencing of the in vitro ALU fragments, no ribosomal depletion was applied.

Bioinformatic Analysis. Quality of the sequenced reads was estimated using FASTQC from the Babraham Institute (Sept. 2016). Adapter trimming using cutadapt and mapping using bwa (aln option – default parameters) were done as described previously (23). The genome assembly used for the alignment was hg19 (Sept. 2016). Conversion of bam files to genomic coordinates was done using bedtools, and subsequently, coordinates of the 5′ end were extracted with in-house scripts. Repeat annotation files were constructed using the filter utility of University of California-Santa Cruz (UCSC) table browser tools against the repeatmasker track of Sept. 2016. Metagene profiles of the read distribution across the ALU sequences were done using the SeqMonk (Babraham Institute) trend probe plots for mapped reads with the same strand with the ALUs. Normalization was done using the relative distribution option. Multiple alignments were performed using EBI Muscle (Edgar, 2004 #164).

ACKNOWLEDGMENTS. We thank all laboratory members for critical discussion. This work was supported by Swiss National Science Foundation Early Postdoc Mobility Fellowship P2LAP3_174617 (to B.B.), and NIH Grant R01-GM090278 and funding from the Howard Hughes Medical Institute (to J.T.L.).

1. E. S. Lander *et al.*; International Human Genome Sequencing Consortium, Initial sequencing and analysis of the human genome. *Nature* **409**, 860–921 (2001).
2. J. C. Venter *et al.*, The sequence of the human genome. *Science* **291**, 1304–1351 (2001).
3. R. H. Waterston *et al.*; Mouse Genome Sequencing Consortium, Initial sequencing and comparative analysis of the mouse genome. *Nature* **420**, 520–562 (2002).
4. P. L. Deininger, J. V. Moran, M. A. Batzer, H. H. Kazazian Jr, Mobile elements and mammalian genome evolution. *Curr. Opin. Genet. Dev.* **13**, 651–658 (2003).
5. S. R. Wessler, Transposable elements and the evolution of eukaryotic genomes. *Proc. Natl. Acad. Sci. U.S.A.* **103**, 17600–17601 (2006).
6. R. Cordaux, M. A. Batzer, The impact of retrotransposons on human genome evolution. *Nat. Rev. Genet.* **10**, 691–703 (2009).
7. A. Hayward, A. Katzourakis, Endogenous retroviruses. *Curr. Biol.* **25**, R644–R646 (2015).
8. W. Dunker, Y. Zhao, Y. Song, J. Karijolich, Recognizing the SINEs of infection: Regulation of retrotransposon expression and modulation of host cell processes. *Viruses* **9**, E386 (2017).

Downloaded at UNIVERSITY OF MASSACHUSETTS on January 9, 2020

9. P. Deininger, Alu elements: Know the SINEs. *Genome Biol.* **12**, 236 (2011).
10. D. A. Kramerov, N. S. Vassetzky, SINEs. *Wiley Interdiscip. Rev. RNA* **2**, 772–786 (2011).
11. K. Singh, M. Carey, S. Saragosti, M. Botchan, Expression of enhanced levels of small RNA polymerase III transcripts encoded by the B2 repeats in simian virus 40-transformed mouse cells. *Nature* **314**, 553–556 (1985).
12. R. Bachvarova, Small B2 RNAs in mouse oocytes, embryos, and somatic tissues. *Dev. Biol.* **130**, 513–523 (1988).
13. J. M. Tucker, B. A. Glaunsinger, Host noncoding retrotransposons induced by DNA viruses: A SINE of infection? *J. Virol.* **91**, e00982-17 (2017).
14. H. Kaneko *et al*., DICER1 deficit induces Alu RNA toxicity in age-related macular degeneration. *Nature* **471**, 325–330 (2011).
15. V. Tarallo *et al*., DICER1 loss and Alu RNA induce age-related macular degeneration via the NLRP3 inflammasome and MyD88. *Cell* **149**, 847–859 (2012).
16. P. Moolhuijzen *et al*., The transcript repeat element: The human Alu sequence as a component of gene networks influencing cancer. *Funct. Integr. Genomics* **10**, 307–319 (2010).
17. B. Kaczkowski *et al*.; FANTOM5 Consortium, Transcriptome analysis of recurrently deregulated genes across multiple cancers identifies new pan-cancer biomarkers. *Cancer Res.* **76**, 216–226 (2016).
18. A. J. Fornace Jr, J. B. Mitchell, Induction of B2 RNA polymerase III transcription by heat shock: Enrichment for heat shock induced sequences in rodent cells by hybridization subtraction. *Nucleic Acids Res.* **14**, 5793–5811 (1986).
19. T. Li, J. Spearow, C. M. Rubin, C. W. Schmid, Physiological stresses increase mouse short interspersed element (SINE) RNA expression in vivo. *Gene* **239**, 367–372 (1999).
20. T. A. Allen, S. Von Kaenel, J. A. Goodrich, J. F. Kugel, The SINE-encoded mouse B2 RNA represses mRNA transcription in response to heat shock. *Nat. Struct. Mol. Biol.* **11**, 816–821 (2004).
21. C. A. Espinoza, T. A. Allen, A. R. Hieb, J. F. Kugel, J. A. Goodrich, B2 RNA binds directly to RNA polymerase II to repress transcript synthesis. *Nat. Struct. Mol. Biol.* **11**, 822–829 (2004).
22. C. A. Espinoza, J. A. Goodrich, J. F. Kugel, Characterization of the structure, function, and mechanism of B2 RNA, an ncRNA repressor of RNA polymerase II transcription. *RNA* **13**, 583–596 (2007).
23. A. Zovoilis, C. Cifuentes-Rojas, H. P. Chu, A. J. Hernandez, J. T. Lee, Destabilization of B2 RNA by EZH2 activates the stress response. *Cell* **167**, 1788–1802.e13 (2016).
24. R. Margueron, D. Reinberg, The polycomb complex PRC2 and its mark in life. *Nature* **469**, 343–349 (2011).
25. J. Zhao, B. K. Sun, J. A. Erwin, J. J. Song, J. T. Lee, Polycomb proteins targeted by a short repeat RNA to the mouse X chromosome. *Science* **322**, 750–756 (2008).
26. S. Kaneko *et al*., Phosphorylation of the PRC2 component Ezh2 is cell cycle-regulated and up-regulates its binding to ncRNA. *Genes Dev.* **24**, 2615–2620 (2010).
27. J. Zhao *et al*., Genome-wide identification of polycomb-associated RNAs by RIP-seq. *Mol. Cell* **40**, 939–953 (2010).
28. S. Kaneko, J. Son, S. S. Shen, D. Reinberg, R. Bonasio, PRC2 binds active promoters and contacts nascent RNAs in embryonic stem cells. *Nat. Struct. Mol. Biol.* **20**, 1258–1264 (2013).
29. C. Cifuentes-Rojas, A. J. Hernandez, K. Sarma, J. T. Lee, Regulatory interactions between RNA and polycomb repressive complex 2. *Mol. Cell* **55**, 171–185 (2014).
30. C. Davidovich *et al*., Toward a consensus on the binding specificity and promiscuity of PRC2 for RNA. *Mol. Cell* **57**, 552–558 (2015).
31. Y. Long *et al*., Conserved RNA-binding specificity of polycomb repressive complex 2 is achieved by dispersed amino acid patches in EZH2. *eLife* **6**, e31558 (2017).
32. Q. Zhang *et al*., RNA exploits an exposed regulatory site to inhibit the enzymatic activity of PRC2. *Nat. Struct. Mol. Biol.* **26**, 237–247 (2019).
33. C. Zhao, A. M. Pyle, Structural insights into the mechanism of group II intron splicing. *Trends Biochem. Sci.* **42**, 470–482 (2017).
34. D. L. Daniels, W. J. Michels Jr, A. M. Pyle, Two competing pathways for self-splicing by group II introns: A quantitative analysis of in vitro reaction rates and products. *J. Mol. Biol.* **256**, 31–49 (1996).
35. K. Y. Lee, B. J. Lee, Structural and biochemical properties of novel self-cleaving ribozymes. *Molecules* **22**, E678 (2017).
36. B. M. Chowrira, J. M. Burke, Extensive phosphorothioate substitution yields highly active and nuclease-resistant hairpin ribozymes. *Nucleic Acids Res.* **20**, 2835–2840 (1992).
37. M. Forconi, D. Herschlag, Use of phosphorothioates to identify sites of metal-ion binding in RNA. *Methods Enzymol.* **468**, 311–333 (2009).
38. S. Basu, S. A. Strobel, Thiophilic metal ion rescue of phosphorothioate interference within the Tetrahymena ribozyme P4-P6 domain. *RNA* **5**, 1399–1407 (1999).
39. J. S. Smith, E. P. Nikonowicz, Phosphorothioate substitution can substantially alter RNA conformation. *Biochemistry* **39**, 5642–5652 (2000).
40. A. Lupták, J. A. Doudna, Distinct sites of phosphorothioate substitution interfere with folding and splicing of the Anabaena group I intron. *Nucleic Acids Res.* **32**, 2272–2280 (2004).
41. M. Hadjiargyrou, N. Delihas, The intertwining of transposable elements and noncoding RNAs. *Int. J. Mol. Sci.* **14**, 13307–13328 (2013).
42. P. D. Mariner *et al*., Human Alu RNA is a modular transacting repressor of mRNA transcription during heat shock. *Mol. Cell* **29**, 499–509 (2008).
43. C. M. Oslowski, F. Urano, Measuring ER stress and the unfolded protein response using mammalian tissue culture system. *Methods Enzymol.* **490**, 71–92 (2011).
44. K. Zhang *et al*., The unfolded protein response transducer IRE1α prevents ER stress-induced hepatic steatosis. *EMBO J.* **30**, 1357–1375 (2011).
45. T. Chatila, L. Silverman, R. Miller, R. Geha, Mechanisms of T cell activation by the calcium ionophore ionomycin. *J. Immunol.* **143**, 1283–1289 (1989).
46. M. Diehn *et al*., Genomic expression programs and the integration of the CD28 costimulatory signal in T cell activation. *Proc. Natl. Acad. Sci. U.S.A.* **99**, 11796–11801 (2002).
47. K. Kruger *et al*., Self-splicing RNA: Autoexcision and autocyclization of the ribosomal RNA intervening sequence of Tetrahymena. *Cell* **31**, 147–157 (1982).
48. C. Guerrier-Takada, K. Gardiner, T. Marsh, N. Pace, S. Altman, The RNA moiety of ribonuclease P is the catalytic subunit of the enzyme. *Cell* **35**, 849–857 (1983).
49. J. Tang, R. R. Breaker, Structural diversity of self-cleaving ribozymes. *Proc. Natl. Acad. Sci. U.S.A.* **97**, 5784–5789 (2000).
50. C. H. Webb, N. J. Riccitelli, D. J. Ruminski, A. Lupták, Widespread occurrence of self-cleaving ribozymes. *Science* **326**, 953 (2009).
51. Z. Weinberg *et al*., New classes of self-cleaving ribozymes revealed by comparative genomics analysis. *Nat. Chem. Biol.* **11**, 606–610 (2015).
52. D. M. J. Lilley, How RNA acts as a nuclease: Some mechanistic comparisons in the nucleolytic ribozymes. *Biochem. Soc. Trans.* **45**, 683–691 (2017).
53. A. Jäschke, Artificial ribozymes and deoxyribozymes. *Curr. Opin. Struct. Biol.* **11**, 321–326 (2001).
54. K. Salehi-Ashtiani, A. Lupták, A. Litovchick, J. W. Szostak, A genomewide search for ribozymes reveals an HDV-like sequence in the human CPEB3 gene. *Science* **313**, 1788–1792 (2006).
55. I. M. Johnson, RNA as a drug target: Recent patents on the catalytic activity of trans-splicing ribozymes derived from group I intron RNA. *Recent Pat. DNA Gene Seq.* **4**, 17–28 (2010).
56. A. Teixeira *et al*., Autocatalytic RNA cleavage in the human beta-globin pre-mRNA promotes transcription termination. *Nature* **432**, 526–530 (2004).
57. M. Martick, L. H. Horan, H. F. Noller, W. G. Scott, A discontinuous hammerhead ribozyme embedded in a mammalian messenger RNA. *Nature* **454**, 899–902 (2008).
58. A. V. Kazantsev *et al*., High-resolution structure of RNase P protein from Thermotoga maritima. *Proc. Natl. Acad. Sci. U.S.A.* **100**, 7497–7502 (2003).
59. G. F. Joyce, G. van der Horst, T. Inoue, Catalytic activity is retained in the Tetrahymena group I intron despite removal of the large extension of element P5. *Nucleic Acids Res.* **17**, 7879–7889 (1989).

Downloaded at UNIVERSITY OF MASSACHUSETTS on January 9, 2020